

Anisotropic electron-distribution function in inverse-bremsstrahlung-heated plasmasA. Bendib,^{1,*} K. Bendib-Kalache,¹ B. Cros,² and G. Maynard²¹*Laboratoire Electronique Quantique, Faculté de Physique, USTHB, Algiers, Algeria*²*Laboratoire de physique des gaz et des plasmas, UMR 8578, Université Paris-Sud 11, Orsay, France*

(Received 18 October 2015; revised manuscript received 22 January 2016; published 25 April 2016)

The electron-distribution function in homogeneous plasmas heated by a high-frequency laser field is calculated in velocity space from the Vlasov-Landau equation. The kinetic model is valid for moderate laser intensity defined by the relevant parameter $\alpha = v_0^2/v_t^2 < 0.5$ where v_0 and v_t are the peak velocity of oscillation in the high-frequency electric field and the thermal velocity, respectively. The results obtained constitute an improvement of the results reported in the literature devoted to weak electric field intensities. The electron-distribution function is calculated solving the kinetic equation with the use of the Legendre polynomial expansion within the laser field dipole approximation. It results in an infinite set of equations for the isotropic component $f_0(v)$ and the anisotropic components $f_{n \geq 1}(v)$ that we have solved numerically with appropriate truncation. For the second anisotropy $f_2(v)$, we found that its maximum increases from the weak electric field intensity ($\alpha < 0.01$) to a moderate one ($\alpha = 0.5$) by a factor $f_{2,\max}(\alpha = 0.5)/f_{2,\max}(\alpha = 0.01) \approx 48$. Applications to the radiation pressure, electromagnetic instabilities, and photoabsorption are also considered.

DOI: [10.1103/PhysRevE.93.043208](https://doi.org/10.1103/PhysRevE.93.043208)**I. INTRODUCTION**

The inverse-bremsstrahlung absorption (IBA) is the most efficient heating mechanism in laser-created plasmas. It corresponds to the absorption of photons by electrons in the presence of electric fields of atoms or ions and the rate of absorption is proportional to the electron-ion (atom) collision frequency. In addition this rate is proportional to the electron-distribution function (EDF) and the slow electrons are preferentially heated by the laser field. The redistribution of the deposited energy by the laser occurs through the electron-electron collisions.

In this area with the kinetic approach, since the pioneering work of Dawson and Oberman [1] and Silin [2] it is well known that the nonlinear IBA of high-frequency electromagnetic waves can result in the modification of the EDF [1–11]. In Ref. [4], Langdon has shown that for the isotropic part of the EDF this modification depends on the relevant parameter Zv_0^2/v_t^2 where $v_0 = \frac{eE_0}{m_e\omega_0}$ is the peak velocity of oscillation in the high-frequency electric field, v_t the thermal velocity, Z the ion charge number, e the electron charge, m_e the electron mass, E_0 the electric field amplitude, and ω_0 the laser frequency. In particular, in homogeneous plasmas, the isotropic part of the EDF is not a Maxwellian but rather a super-Gaussian [6] which varies as $\exp[-(v/v_m)^m]$ where v_m is a characteristic velocity and m is a parameter which depends on Zv_0^2/v_t^2 . It varies from $m = 2$ for $Zv_0^2/v_t^2 \ll 1$ to $m = 5$ for $Zv_0^2/v_t^2 \gg 1$ while respecting the linear condition $\alpha = v_0^2/v_t^2 \ll 1$. As a result, for m varying from 2 to 5, absorption is reduced by up to a factor of 2. Besides, several physical processes may be altered by the Gaussian shape of the EDF such as the continuum x-ray emission [6], the Weibel instability [11], and the spectrum of electron plasma wave fluctuations [10].

In this work we propose a kinetic model to investigate the deformation of the anisotropic part of the EDF due to the IBA for a moderate range of laser intensity such as

$\alpha < 0.5$. This condition is discussed below and it allows us to use the isotropic distribution function established in earlier work [4,6,10]. For $\alpha > 0.5$ both isotropic and anisotropic parts of the EDF have to be considering on equal footing and should be calculated self-consistently. This strongly nonlinear regime is beyond the scope of this work.

For the anisotropic part of EDF, the linear regime ($\alpha \ll 1$) was examined [7] to identify a new source for the electromagnetic instabilities driven by EDF anisotropy induced by the IBA. Note that by “linear regime” we mean that the isotropic part of the EDF is a Maxwellian and the anisotropic part [7] depends linearly on alpha (or the laser intensity). This work constitutes an extension of this previous work [7] to moderate nonlinear range $\alpha < 0.5$ and, also, it complements the works reported in the literature devoted only to the isotropic EDF in laser-heated plasmas. Typically, for $\alpha > 0.01$ the nonlinear effects have to be accounted for and such plasmas are those created by high laser intensities which in turn will induce important physical processes. Our kinetic model is limited to classical underdense ($\omega \leq \omega_p$) plasmas with electron temperature such that α is not too small compared to 1 (a few tenths of 1). Potential applications of our results include the generation of ultrashort intense pulses by Raman amplification [12], the guiding of high-intensity laser pulses in a plasma filled capillary tube [13], the IBA of electromagnetic radiation in anisotropic plasmas [14], and photoionization, bremsstrahlung, and radiative recombination emissions [6,15,16], etc.

This work is organized as follows. In Sec. II we present the kinetic model equations based on the Vlasov-Landau equation. Section III is devoted to the numerical computation of the low-frequency EDF altered by the high-frequency electromagnetic field. Then, the next section deals with three applications: the computation of the radiation pressure, the stability analysis of the electromagnetic modes beyond the linear regime, and the effects of the modification of the EDF on the IBA. We summarize the main results obtained in this work in the last section.

*mbendib@hotmail.com

II. LOW-FREQUENCY VLASOV-LANDAU EQUATION

The starting equation for the EDF is Vlasov's equation, which in 1938, he adapted from the Fokker-Planck equation for Brownian motion of 1914–1915. The plasma is assumed homogeneous and in the presence of a high-frequency electric field; in these conditions this equation reads

$$\frac{\partial f}{\partial t} - \frac{e}{m}(\vec{E} + \vec{v} \times \vec{B}) \cdot \frac{\partial f}{\partial \vec{v}} = C_{ei}(f) + C_{ee}(f), \quad (1)$$

where $f(\vec{v}, \vec{r}, t)$ is the EDF, \vec{E} and \vec{B} are the electric and magnetic fields, and e and m are the electron charge and the electron mass, respectively. The first term on the right-hand side of Eq. (1) is the electron-ion Landau collision term

$$C_{ei}(f) = \frac{v_t^4}{2\lambda_{ei}v^3} \frac{\partial}{\partial v_i} (v_i v_j - v^2 \delta_{ij}) \frac{\partial f}{\partial v_j}, \quad (2)$$

where $\lambda_{ei} = \frac{4\pi\epsilon_0^2 T^2}{ne^4(Z+1)\ln\Lambda}$ is the electron mean free path, Z is the ion charge number, T is the electron temperature (in energy units), n is the electron density, and $\ln\Lambda$ is the Coulomb logarithm. We should note that for simplicity the electron-electron collision term $C_{ee}(f)$ in Eq. (1) is not accounted for in our model. The e - e collision term is a complex integrodifferential operator and this makes difficult the solution of the Fokker-Planck equation. Nevertheless for $Z \gg 1$ the approximation $C_{ee}(f) \ll C_{ei}(f)$ is fulfilled in the anisotropic part of Eq. (1). In addition it is well known that strong electromagnetic fields could modify the electron-ion Coulomb scattering [17–21]. For a full summary of existing theories we refer the reader to Ref. [19]. We mention that in the intermediate nonlinear range considered in this work this dependence is negligible as shown in Fig. 11 of Ref. [19].

As it stands Eq. (1) is not easy to handle. To solve it we use the high- and low-frequency splitting, i.e., $f = f_s + f_h$, $\vec{E} = \vec{E}_h$, and we readily obtain

$$\frac{\partial f_s}{\partial t} - \frac{e}{m} \left\langle \vec{E}_h \cdot \frac{\partial f_h}{\partial \vec{v}} \right\rangle = C_{ei}(f_s), \quad (3)$$

$$\frac{\partial f_h}{\partial t} - \frac{e}{m} \vec{E}_h \cdot \frac{\partial f_s}{\partial \vec{v}} = C_{ei}(f_h), \quad (4)$$

where the subscripts s and h stand, respectively, for low and high frequency and the brackets in (3) indicate the average over the high-frequency field period $T = 2\pi/\omega_0$. The high-frequency terms are written as $\vec{E}_h = \text{Re}[E_0 \exp(-i\omega_0 t)]\hat{x}$ and $f_h(\vec{v}, t) = \text{Re}[\tilde{f}_h(\vec{v}, t) \exp(-i\omega_0 t)]$ where a linearly polarized laser wave along the x axis is adopted and the amplitudes $E_0(t)$ and $\tilde{f}_h(\vec{v}, t)$ are assumed slowly varying with time. From Eqs. (3) and (4) the low-frequency EDF equation was derived in Ref. [7]. The method consists first from Eq. (4), to calculate iteratively $f_h(\vec{v}, t)$ as a function of f_s with the use of the ordering $\omega_0 \gg \nu_{ei}$ where $\nu_{ei} = v_t/\lambda_{ei}$ is the electron collision frequency,

$$f_h \approx -\frac{ie}{m_e\omega_0} \vec{E}_h \cdot \frac{\partial f_s}{\partial \vec{v}} - \frac{e}{m_e\omega_0^2} C_{ei} \left(\vec{E}_h \cdot \frac{\partial f_s}{\partial \vec{v}} \right). \quad (5)$$

Then, substituting (5) into (3) we obtain the secular kinetic equation. We assume as in Ref. [7] a negligible time evolution of the anisotropic part of EDF; i.e., the IBA is balanced

by the electron-ion diffusion in the velocity space. Here we present the results in appropriate form for the purpose of numerical computations with the use of the expansion on the Legendre polynomial basis, $f_s(\vec{v}) = \sum_{n=0}^{\infty} P_l(\mu) f_n(v)$, where $\mu = \cos\theta = \frac{\vec{E}_h \cdot \vec{v}}{E_h v}$ and $P_n(\mu)$ is the Legendre polynomial of order n ,

$$\begin{pmatrix} f_2'' \\ f_4'' \\ \dots \\ f_l'' \\ \dots \end{pmatrix} = y^{-1} (F_{ij}'')^{-1} F_{ij}^1 \begin{pmatrix} f_2 \\ f_4 \\ \dots \\ f_l \\ \dots \end{pmatrix} + y^{-2} (F_{ij}'')^{-1} F_{ij}^2 \begin{pmatrix} f_2 \\ f_4 \\ \dots \\ f_l \\ \dots \end{pmatrix} \\ + y^{-1} (F_{ij}'')^{-1} F_{ij}' \begin{pmatrix} f_2' \\ f_4' \\ \dots \\ f_l' \\ \dots \end{pmatrix} \\ + y^{-1} (F_{ij}'')^{-1} S_{ij}^0 \begin{pmatrix} y^{-1} f_0 \\ f_0' \\ y f_0'' \\ 0 \\ \dots \end{pmatrix}, \quad (6)$$

where

$$F_{ij}'' = \begin{pmatrix} b_2 & c_2 & 0 & \dots & \dots & \dots \\ a_4 & b_4 & c_4 & 0 & \dots & \dots \\ \dots & \dots & \dots & \dots & \dots & \dots \\ 0 & 0 & a_l & b_l & b_l & 0 \\ \dots & \dots & \dots & \dots & \dots & \dots \end{pmatrix}, \quad (7)$$

$$F_{ij}' = \begin{pmatrix} 0 & L_2 & 0 & \dots & \dots & \dots \\ J_4 & 0 & L_4 & 0 & \dots & \dots \\ \dots & \dots & \dots & \dots & \dots & \dots \\ 0 & 0 & J_l & 0 & L_l & \dots \\ \dots & \dots & \dots & \dots & \dots & \dots \end{pmatrix}, \quad (8)$$

$$F_{ij}^1 = \begin{pmatrix} I_2^1 & 0 & \dots & \dots & \dots & \dots \\ 0 & I_4^1 & 0 & \dots & \dots & \dots \\ \dots & \dots & \dots & \dots & \dots & \dots \\ \dots & \dots & 0 & I_l^1 & 0 & \dots \\ \dots & \dots & \dots & \dots & \dots & \dots \end{pmatrix}, \quad (9)$$

$$F_{ij}^2 = \begin{pmatrix} I_2^2 & M_2 & 0 & \dots & \dots & \dots \\ K_4 & I_4^2 & M_4 & 0 & \dots & \dots \\ \dots & \dots & \dots & \dots & \dots & \dots \\ \dots & 0 & K_l & I_l^2 & M_l & \dots \\ \dots & \dots & \dots & \dots & \dots & \dots \end{pmatrix}, \quad (10)$$

$$S_{ij}^0 = \begin{pmatrix} K_2 & J_2 & -a_2 & 0 & \dots \\ 0 & 0 & 0 & 0 & 0 \\ \dots & \dots & \dots & \dots & \dots \end{pmatrix}. \quad (11)$$

The dash in Eq. (6) denotes the derivative order with respect to the dimensionless variable $y = v^2/2v_t^2$ and the coefficients in Eqs. (7)–(11) are defined as follows:

$$a_l = \frac{v_0^2}{v_t^2} \frac{l^2(l-1)^2}{(2l-1)(2l-3)}, \quad (12)$$

$$b_l = \frac{v_0^2}{v_t^2} \frac{1}{(2l+1)} \left[\frac{l^3(l-1)}{(2l-1)} + \frac{(l+1)^3(l+2)}{(2l+3)} \right], \quad (13)$$

$$c_l = \frac{v_0^2 (l+1)^2 (l+2)^2}{v_i^2 (2l+3)(2l+5)}, \quad (14)$$

$$I_l^1 = l(l+1), \quad (15)$$

$$I_l^2 = \frac{v_0^2}{v_i^2} \frac{1}{4(2l+1)} \left[\frac{l^3(l^2-1)(l+3)}{(2l-1)} + \frac{l(l+1)^3(l^2-4)}{(2l+3)} \right], \quad (16)$$

$$J_l = \frac{v_0^2 l^2 (l-1)^2}{v_i^2 2(2l-3)}, \quad (17)$$

$$K_l = -\frac{v_0^2 l^2 (l-1)^2 (l-2)(l+3)}{v_i^2 4(2l-1)(2l-3)}, \quad (18)$$

$$L_l = -\frac{v_0^2 (l+1)^2 (l+2)^2}{v_i^2 2(2l+5)}, \quad (19)$$

$$M_l = -\frac{v_0^2 (l+1)^2 (l+2)^2 (l+3)(l-2)}{v_i^2 4(2l+3)(2l+5)}. \quad (20)$$

To be more complete we should add the isotropic equation

$$\frac{\partial f_0}{\partial t} - \frac{e}{2m_e} \text{Re} \left(E_0 \frac{\sqrt{2}}{3v_i v_l^{1/2}} \frac{\partial y f_{h1}}{\partial y} \right) = C_{ee}(f_0), \quad (21)$$

where f_{h1} is the first anisotropy of the high-frequency EDF expanded on the Legendre polynomial basis. Here we mention that Eq. (6) is derived for collisional plasmas but it does not contain the expression of the collision frequency ν_{ei} . This is due to the balance between electron-ion collisions which tend to make the EDF isotropic and the IBA which tends to make the EDF anisotropic.

We can see that in the anisotropic part of the Vlasov-Landau equation (6) the relevant parameter is $\alpha = v_0^2/v_i^2$. This parameter quantifies the importance of the plasma anisotropy induced by collisional absorption of laser energy by electrons oscillating along the electric field direction. Thus the greater α is, the higher is the degree of plasma anisotropy. In the isotropic equation (21) there is a competition between the electron-electron collision term proportional to $\nu_{ee}v_i^2 \sim \nu_{ei}v_i^2/Z$ which tends $f_0(v)$ to a Maxwellian, and the collisional absorption term proportional to $\nu_{ei}v_0^2$ which tends to modify the form of $f_0(v)$. As shown by Langdon [4] the relevant parameter is thus $Z\alpha = Zv_0^2/v_i^2$; for $Z\alpha \ll 1$, $f_0(v)$ is very close to a Maxwellian while for $Z\alpha \gg 1$, it behaves as a super-Gaussian $\sim u^{-3} \exp(-v^5/5u^5)$, where $u = (\frac{5v_i^4 v_0^2}{12\lambda_{De}^2} t)^{1/5}$ is a characteristic velocity. A numerical solution of Eq. (21) was derived by Matte *et al.* in Ref. [6]. The authors proposed an accurate numerical fit of $f_0(v)$ that we used in this work, and which is valid for arbitrary values of $Z\alpha$,

$$f_0(v) = \frac{n}{4\pi} \frac{m}{\Gamma(3/m)v_m^3} \exp(-(v/v_m)^m), \quad (22)$$

with

$$m(Z\alpha) = 2 + 3/[1 + 1.66/(Z\alpha)^{0.724}], \quad (23)$$

$$v_m^2 = \frac{3T}{m_e} \frac{\Gamma(3/m)}{\Gamma(5/m)}, \quad (24)$$

where $\Gamma(x)$ is the Euler Gamma function. We should note that the hydrodynamics of the plasma is defined by a constant

background density, the plasma is at rest, and its temperature depends on time since it is heated by IBA. So implicitly in Eqs. (22) and (24) the temperature is a time-dependent function, $T = T(t)$, and its evolution is governed by the energy equation

$$\frac{3}{2}n \frac{\partial T}{\partial t} = \frac{2\pi}{3} \frac{v_i^4}{\lambda_{ei}} m v_0^2 f_0(0), \quad (25)$$

that we have to couple with the kinetic equation. In addition the analytic self-similar isotropic EDF calculated in the limit $Z\alpha \gg 1$ depends explicitly on λ_{ei} while the numerical fit (22) does not depend on λ_{ei} explicitly but only through the energy equation (25).

We can see that Eq. (6) can be split into two independent blocks of equations defined by odd ($l = 2n - 1$) and even ($l = 2n$) orders where $n \geq 1$ is an integer number. For the odd order, we obtain a set of homogeneous equations to which the obvious solution is, whatever n , $f_{2n-1}(v) = 0$. For the even order, Eq. (6) is an inhomogeneous system of infinite coupled ordinary differential equations (ODEs) that we have solved with respect to the variable $v/\sqrt{2}v_i$. To solve this system of equations we perform a truncation at a given order $l_{\max} = 2n_{\max}$ and to be self-consistent, we consider $f_{l > 2n_{\max}}(v) = 0$. Each equation is a second-order ODE with variable coefficients which does not admit an obvious solution for arbitrary values of α . However, for weak laser intensity or large temperature, corresponding to the approximation $\alpha \ll 1$, the higher anisotropies $f_{l \geq 4}$ are negligible and an analytic solution for f_2 was found in Ref. [7],

$$f_2(y) = \frac{v_0^2}{v_i^2} \left(\frac{1}{3} + \frac{2y}{9} \right) f_0. \quad (26)$$

III. NUMERICAL RESULTS

In this work we solved numerically the even-order set of equations for moderate values of α with the use of the finite difference scheme and the lower and upper boundary conditions $\frac{df_{2n}}{dv}(0) = 0$ and $\frac{df_{2n}}{dv}(v_{\max}) = 0$, respectively. The lower boundary condition is motivated by the exact analytical solution (26) which verifies this condition. Furthermore, let us consider a bi-Maxwellian EDF $f_{bM}(v, T_x, T_\perp)$ defined by the two temperatures T_x and T_\perp . We can readily deduce the expression of the second anisotropy, $f_2 = \frac{1}{\sqrt{5}} \frac{mv^2}{2T} \frac{\Delta T}{T} \exp(-mv^2/2T)$ where $T = T_x - \Delta T$ is the isotropic temperature and $\Delta T = \frac{2}{3}(T_x - T_\perp)$. We can see again that the condition $\frac{df_2}{dv}(0) = 0$ is well fulfilled by this standard anisotropic EDF. Concerning the upper boundary condition at $v = v_{\max}$, both conditions $\frac{df_{2n}}{dv}(v_{\max}) = 0$ and $f_{2n}(v_{\max}) = 0$ work and give the same numerical results. We note that in the numerical applications we set $v_{\max} = 40v_i$. The ion charge number is $Z = 13$ that we used throughout this work.

To solve the system of equations (6) with any fixed α , the problem of convergence of the solution arises. Our approach consists first to solve the equations with a fixed l_{\max} . Then we perform the numerical calculations with $l_{\max} + 1$ and compare the results obtained for the second anisotropy, $f_2(l_{\max})$ and $f_2(l_{\max} + 1)$, respectively. We consider that the results are sufficiently accurate if the two results are close within a precision of 5%. We mention that this numerical method

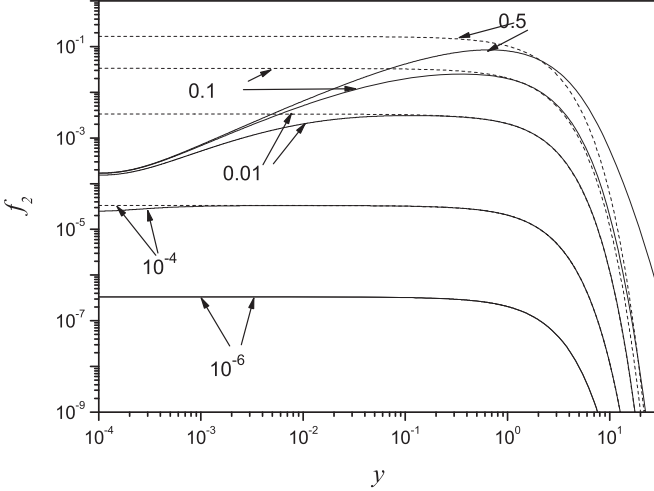


FIG. 1. Second anisotropy $f_2(y)$ as a function of the normalized square velocity $y = v^2/2v_t^2$ for $\alpha = 10^{-6}$, 10^{-4} , 10^{-2} , 0.1, and 0.5. The dashed curve corresponds to the analytical expression (26).

exhibits a rapid convergence and the higher α is, the higher is l_{\max} .

We give in Fig. 1 the numerical solution for the second anisotropy $f_2(y)$ for different values of α . This simulation is performed with $n_{\max} = 5$ and the normalized Maxwellian $f_0(y) = \exp(-y)$. The analytical solution (26) is also represented. The excellent agreement between the analytical and numerical solutions can be noted for $\alpha = 10^{-6}$. When α increases the numerical solution exhibits a departure from the asymptotic behavior of the analytical solution for $y \rightarrow 0$. This difference becomes important for $\alpha = 0.1$ used in applications in Refs. [7] and [17]. However, it does not call into question the results obtained in these works since rather it is the moments $M_2^x = \int_0^\infty y^x f_2(y) dy$ with $x \geq 1/2$ which are used in the stability analysis of the electromagnetic modes. Indeed, for instance, calculating this moment for $x = 1/2$, we obtained 0.06 and $0.1\sqrt{\pi}/3 \approx 0.059$, respectively, for the numerical and the analytical solutions. For $\alpha = 0.5$ and the typical electron velocity $y_{\max} \approx 0.71$, the departure is about 32%. This departure increases for increasing α and it is only due to the contribution of higher anisotropies $f_4 - f_{10}$ to the second anisotropy f_2 since f_0 is kept Maxwellian.

In Fig. 2 we present the numerical results for f_2 with the numerical fit (22) and for various values of α (10^{-4} , 10^{-2} , 0.3, 0.5). The results clearly show that the maximum of $f_2(y)$ increases as α increases. It increases from $f_{2\max} \approx 0.0027$ in the linear regime ($\alpha = 0.01$) to $f_{2\max} \approx 0.133$ in the moderate nonlinear regime ($\alpha = 0.5$). Furthermore, y_{\max} increases with increasing α , and thus we expect that the high-order moments of the second anisotropy increase quickly with α . To investigate the role of the parameter α on the induced plasma anisotropy through the isotropic EDF $f_0(y)$, we display also the numerical results with a Maxwellian. We can see that the deformation of the isotropic EDF, $f_0(y)$, by the IBA changes significantly, $f_2(y)$. In the range $0.5v_t < v < 2v_t$ a negligible deviation for $\alpha = 10^{-4}$ can be observed; however, the departure is about 14% for $\alpha = 10^{-2}$, and about 40% for $\alpha = 0.5$.

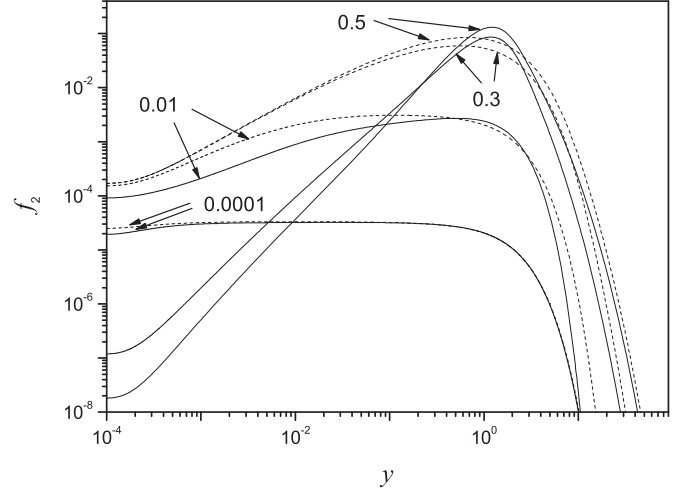


FIG. 2. Second anisotropy $f_2(y)$ for $\alpha = 10^{-4}$, 10^{-2} , 0.3, and 0.5 as a function of $y = v^2/2v_t^2$. The simulation is performed with the numerical fit (22) for the solid lines and a Maxwellian for the dashed lines.

It is well known that the second anisotropy corresponds at the macroscopic level to the electron temperature anisotropy. Here the temperature anisotropy is induced by the absorption of the laser energy preferentially along the high-frequency electric field direction (x axis). It results in two temperatures, T_x along the x axis greater than the isotropic temperature T , and T_\perp in the perpendicular direction, smaller than T . From the standard definition of the temperature we express T_x as $T_x = T + \Delta T = T(1 + M_2^{3/2}/\sqrt{5\pi})$. For $\alpha = 0.3$ we found $\Delta T/T \approx 8 \times 10^{-2}$. It follows that T_x and T_\perp are close within roughly 10%. Thus it can be considered that the laser energy is absorbed mainly by isotropic temperature plasmas. The IBA in plasmas with temperature anisotropy is treated, for instance, in Ref. [14] with the use of a bi-Maxwellian.

In Fig. 3 we report the numerical results for the first two higher anisotropies, $f_4(y)$ and $f_6(y)$, with $\alpha = 0.5$.

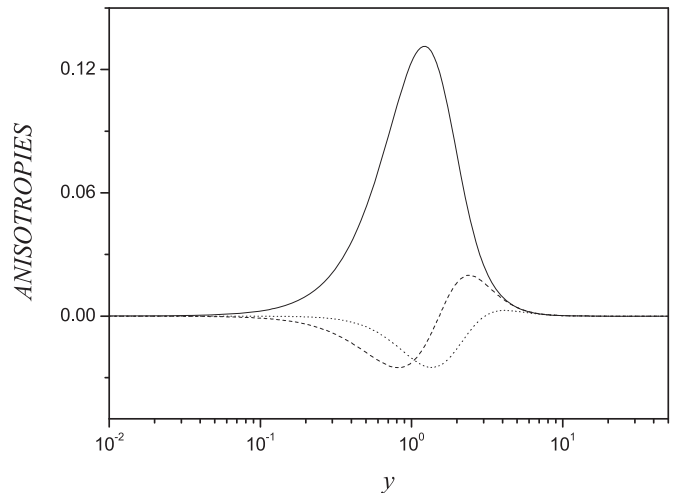


FIG. 3. Second anisotropy (solid line) and higher anisotropies $f_4(y)$ (dashed line) and $f_6(y)$ (dotted line) as a function of $y = v^2/2v_t^2$ for $\alpha = 0.5$.

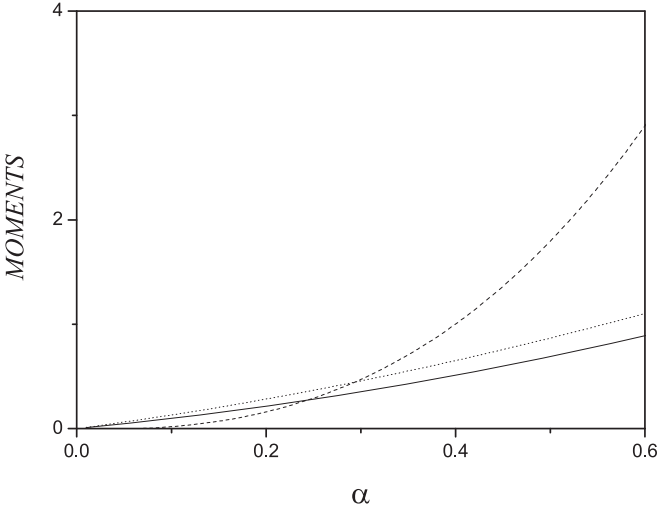


FIG. 4. Moments $M_2^{3/2}$ calculated with the numerical fit (22) (solid line) and a Maxwellian (dotted line) as a function of α . The dashed line corresponds to the moment $M_4^{5/2}$.

We observe that the higher anisotropies are not negligible since $f_{2\max}/f_{4\max} \sim 6.5$. These results confirm, as shown in Fig. 1, that they play an important role in the deformation of $f_2(y)$. The anisotropies $f_{i \geq 2}(y)$ define high hydrodynamic moments in the fluid equations such as $P_{ij} = \int_{-\infty}^{+\infty} m v_i v_j f(v) d\vec{v}$ for $f_2(y)$, and $R_{ijkl} = \int_{-\infty}^{+\infty} m v_i v_j v_k v_l f(v) d\vec{v}$ for $f_4(y)$. In the present geometry of the problem they correspond to the normalized moments $P_{xx} \sim M_2^{3/2} = \int_0^\infty y^{3/2} f_2(y) dy$ and $R_{xxxx} \sim M_4^{5/2} = \int_0^\infty y^{5/2} f_4(y) dy$, respectively. The moment of the second anisotropy plays a crucial role in the stability analysis of the quasistatic electromagnetic modes [7,22–24] since it constitutes the driven term of the instability. We give in Fig. 4 the moment $M_2^{3/2}$ as a function of α (solid line). For weak values of α we have checked that the analytic solution $M_2^{3/2} = \frac{2\sqrt{\pi}}{3}\alpha$ derived from Eq. (26) is recovered. In particular we found in this limit the component x - x of the strain tensor $P_{xx} = \frac{8}{15} m n v_0^2$, derived in Ref. [9] with the perturbation approach and in Ref. [25] with Chapman-Enskog formalism. We note that the moment $M_2^{3/2}$ normalized to α increases slowly. For instance, $\frac{M_2^{3/2}(\alpha=0.5)}{0.5} / \frac{M_2^{3/2}(\alpha=0.01)}{0.01} \approx 2.9$. To estimate the role of the parameter $m(Z\alpha)$ on the moments of the anisotropic EDF we presented (dotted line) the moment $M_2^{3/2}$ with a Maxwellian. It may be noted that for $\alpha = 0.5$ the difference between the two results is about 26%; we conclude thus that the deformation of $f_0(v)$ by the IBA should significantly influence the anisotropic moments. For the higher moment $M_4^{5/2}$ (dashed line) it increases more rapidly with α and in the range ($\alpha < 0.1$) it is negative. This trend should be fulfilled for high-order moments.

A second application concerns the stability analysis of the electromagnetic instabilities [23] in the collisionless regime. Schematically the mechanism for these microinstabilities can be modeled by the formation of perturbed currents by a seed of quasistatic magnetic field. In appropriate physical conditions where the plasma presents a nonvanishing second anisotropic EDF, this current in turn produces a self-consistent

magnetic field increasing the original field at the expense of the plasma free energy. In the collisionless regime the collective mechanisms (Landau damping) tend to stabilize the instability. The competition between the non-thermal free energy and the stabilizing mechanisms are relevant in the excitation of such instabilities. Generally the description of the electromagnetic instability does not account for the feedback of the B field on the driven term and the instability rapidly grows in amplitude without being switched off. In the collisionless limit the dispersion relation of this instability is derived in Refs. [11] and [24] and the growth rate reads

$$\gamma = -\frac{2\sqrt{3}}{\pi} \frac{[\Gamma(\frac{3}{m})]^{3/2}}{\Gamma(\frac{2}{m})[\Gamma(\frac{5}{m})]^{1/2}} (k v_t)^3 \left(\frac{c}{\omega_p v_t}\right)^2 + \frac{2\sqrt{2}}{3\pi} \frac{m\Gamma(\frac{5}{m})}{\Gamma(\frac{3}{m})\Gamma(\frac{2}{m})} k v_t M_2^{1/2}, \quad (27)$$

where c is the speed of light, ω_p the plasma frequency, and k the wave number of the electromagnetic mode. For this instability induced by the IBA, the group velocity is negligible [24] and the unstable modes do not suffer convection away from the excitation region but rather they grow locally. From Eq. (27) the most unstable mode is given by the optimum wave number,

$$k_{\text{opt}} = \left\{ \frac{\sqrt{2}}{9\sqrt{3}} \frac{m[\Gamma(\frac{5}{m})]^{3/2}}{[\Gamma(\frac{3}{m})]^{5/2}} \left(\frac{v_t}{c}\right)^2 M_2^{1/2} \right\}^{1/2} \frac{\omega_p}{v_t}, \quad (28)$$

and the corresponding maximum growth rate is

$$\gamma_{\text{max}} = \frac{4\sqrt{2}}{9\pi} \frac{m\Gamma(\frac{5}{m})k_{\text{opt}}v_t}{\Gamma(\frac{3}{m})\Gamma(\frac{2}{m})} M_2^{1/2}. \quad (29)$$

For typical plasma and laser parameters, $n \approx 9.8 \times 10^{20} \text{ cm}^{-3}$, $T = 4 \text{ keV}$, and $\alpha = 0.3$, we obtain $\gamma \approx 5 \times 10^{12} \text{ s}^{-1}$. The collisionality parameter is about $k_{\text{opt}}\lambda_{ei} \approx 12$ and this justifies the collisionless approximation used to derive Eq. (27). Thus for moderate laser intensity corresponding to moderate electron temperature anisotropy ($\Delta T/T \approx 8 \times 10^{-2}$), strongly growing Weibel modes driven by IBA are found. These results do not account for the stabilizing term [22] in the dispersion relation due to the feedback of the driven B field on the instability. In addition, in Ref. [7] the stability analysis of electromagnetic modes driven by IBA shows that the most unstable modes take place in the semicollisional range. More quantitative results on the stability analysis of electromagnetic modes in laser-created plasmas need more work. It is beyond the scope of the present paper and it will be done in a future work.

The last application deals with the influence of non-Maxwellian EDF on the photoabsorption. Some authors [6,15,16] have studied the emissivity coefficients (bremsstrahlung and radiative recombination) in plasmas in the presence of a strong electric field. In light of our numerical results, we propose an application which extends this investigation to the central process studied in this work, the photoabsorption. More precisely, we estimate the role of nonlinear effects due to intense laser field on the frequency-dependent absorption cross section. For strongly transparent plasmas the energy absorption coefficient per unit time and

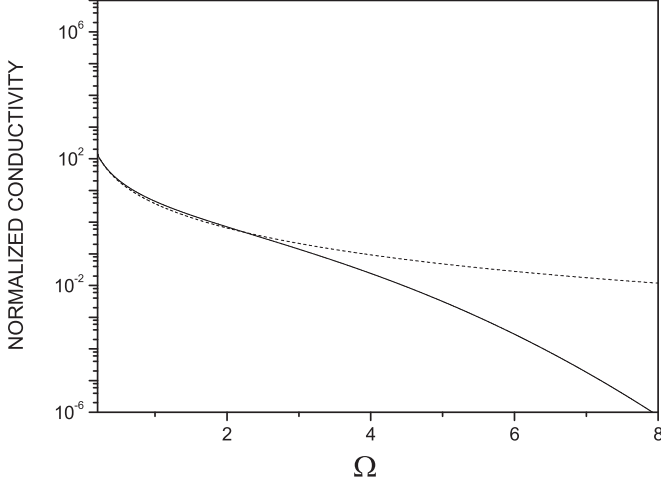


FIG. 5. Normalized conductivity $\sigma / \left[\frac{n_e e^2 \hbar^2}{m_e T^2} \frac{n_e}{Z v_i^3} \left(\frac{Z e^2}{4 \pi \epsilon_0 m_e} \right)^2 \right]$ as a function of $\Omega = \frac{\hbar \omega}{T}$ for $\alpha \ll 1$ (dashed line) corresponding to the thermal equilibrium and $\alpha = 0.5$ (solid line).

per unit length A is defined by the real part of the high-frequency conductivity σ as $A = \sigma / c \epsilon_0$, where ϵ_0 is the vacuum permittivity. The IBA is thus associated with the conductivity defined with the use of the Kirchhoff laws by

$$\sigma = S \frac{\pi^2 \hbar \epsilon_0 c^3}{(\hbar \omega / T)^2 T^3} \left[\frac{\exp\left(\frac{\hbar \omega}{T}\right) - 1}{\frac{\hbar \omega}{T}} \right], \quad (30)$$

where

$$S = \frac{16 \pi \alpha^3 \hbar^3 n_e n_i Z^2}{3 \sqrt{3} m_e^2} \int_{v_{\min} = \sqrt{\frac{2 \hbar \omega}{m_e}}}^{\infty} G(\omega, v) f_0(v) v dv \quad (31)$$

is the power spectrum per unit volume emitted by bremsstrahlung, $\alpha = \frac{e^2}{4 \pi \epsilon_0 \hbar c}$ is the fine-structure constant, \hbar is the reduced Planck's constant, and $G(\omega, v)$ the Gaunt factor approximated to 1 for $\omega \gg \omega_p$. We give in Fig. 5 the spectrum of the normalized conductivity for $\alpha \ll 1$ (thermal equilibrium) and $\alpha = 0.5$. The deformation of the EDF leads to a strong reduction of the conductivity in the spectral range $\hbar \omega / T_e > 2.4$. For low electron energy $\hbar \omega / T_e \ll 1$, the last factor in Eq. (30) is close to one and we recover the behaviour $\sigma \sim \omega^{-2}$ as the high-frequency conductivity derived from the Fokker-Planck equation. We note that in this low-energy range the non-Maxwellian effects on the absorption rate are weak and both Maxwellian and non-Maxwellian results are comparable. We should note that for frequency ω smaller than or of the same order as the plasma frequency ω_p , the two-body description is no longer adequate and the full Fokker-Planck equation treatment is required.

Let us now discuss the validity of our model. To use the numerical fit (22) it is important to study its validity beyond the nonlinear regime ($\alpha > 0.01$). For this we refer to the high-frequency equation used by Langdon (Eq. (3) in Ref. [4]),

$$\frac{\partial f_{1hf}}{\partial t} + \frac{e E_{hf}}{m} C_1 = -\frac{v_t^4}{\lambda_{ei} v^3} f_{1hf} + C_{ee}(f_{1hf}), \quad (32)$$

where $C_1 = -\frac{\partial f_0}{\partial v} - \frac{2}{5 v^3} \frac{\partial}{\partial v} (v^3 f_2)$. Equation (22) was obtained by neglecting, in C_1 , the term proportional to f_2 , which is

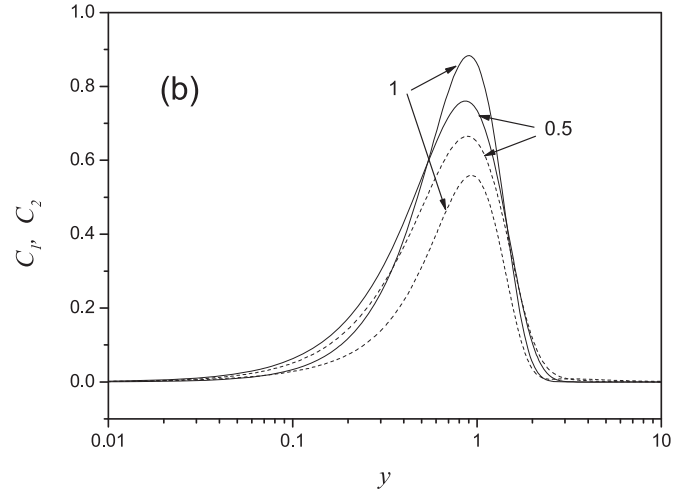
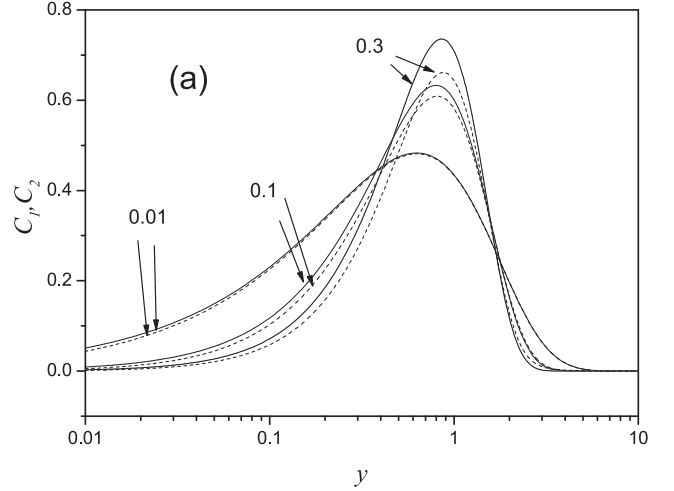


FIG. 6. Coefficient $C_1(v) = -\frac{\partial f_0}{\partial v} - \frac{2}{5 v^3} \frac{\partial}{\partial v} (v^3 f_2)$ (dashed line) and $C_2(v) = -\frac{\partial f_0}{\partial v}$ (solid line) as a function of $y = v^2 / 2 v_i^2$ for various values of α .

justified for $Z v_0^2 / v_i^2 \ll 1$. By using (22), we must verify after calculating f_2 that the condition $-\frac{\partial f_0}{\partial v} \gg -\frac{2}{5 v^3} \frac{\partial}{\partial v} (v^3 f_2)$ is satisfied. We calculated numerically C_1 and $C_2 = -\frac{\partial f_0}{\partial v}$ in order to compare their magnitude; the results are shown in Fig. 6 for different values of α . It may be noted that for $\alpha < 0.1$ both coefficients C_1 and C_2 are very close. For $\alpha < 0.3$ we found that the difference is less than 10% and for $\alpha < 0.5$, it is less than 13%. We can see that the departure between the two results obtained with the coefficients C_1 and C_2 is not important. This allows us to conclude that the numerical fit (22) can be used with confidence for the intensity range $\alpha < 0.5$. On the other hand we expect that beyond this moderate range of intensities ($\alpha > 0.5$) the problem must be solved self-consistently, since for $\alpha = 1$, the difference is about 40%.

The main result obtained in this work is the generation of a second anisotropy in the EDF under the influence of electromagnetic fields. We have found that this anisotropy could play an important role since it is responsible for the generation of a strong quasistatic magnetic field in the megagauss range and of a radiative force comparable to the ponderomotive force. Both

effects can affect electron dynamics, transport properties, and growth rates of instabilities driven in such plasmas. The other consequence of the nonlinear effects induced by intense laser fields is the reduction of the emissivity coefficients and the photoabsorption due to the flat-topped EDF built by the IBA and to the high-velocity anisotropy.

We should note that for the IBA, the quantum relativistic domain is now opened up and in the literature several works are devoted to such regimes. We refer the reader to the recent work of Avetissian *et al.* [26], where nonlinear IBA of an intense x-ray laser field in the dense classical and quantum plasmas is investigated with the use of the Liouville–von Neumann equation for the density matrix. Their analytical and numerical applications are presented for both classical (Maxwellian EDF) and degenerate plasmas (Fermi-Dirac EDF). The relativistic effects are also included in the model through the electron relativistic oscillations in strong electric fields. The effects of untraintense electric field on the EDF itself, which needs a kinetic theory treatment, are not accounted for. Our results are restricted to classical plasmas; they can be extended to relativistic plasmas with electron thermal energy comparable to the rest energy $m_e c^2$. This extension is in order and will be submitted in a future work. Note that Avetissian *et al.* [27] have investigated this relativistic regime with the Jütner-Maxwell-Boltzmann EDF to calculate the absorption coefficient of the electromagnetic wave with arbitrary polarization and intensity.

IV. SUMMARY

The anisotropic part of EDF $f_{an}(\vec{v})$ in laser-heated plasmas is calculated from the Vlasov-Landau equation for

moderate strength of the peak velocity of oscillation in the high-frequency electric field. The deformation of the EDF is produced under the influence of IBA and electron-ion collisions. This work complements previous studies [4,6,10] devoted to the behavior of the isotropic EDF $f_0(v)$ with respect to the parameter $Z\alpha$. It has been shown that for $\alpha > 0.01$ the modification of the anisotropic part of EDF has to be accounted for. The deformation of $f_2(v)$ due to the IBA is related to the deformation of the symmetric EDF $f_0(v)$ and high anisotropies $f_{2n \geq 4}(v)$ for $\alpha < 0.5$. The first application of the numerical results is devoted to the moment of the second anisotropy which defines the stress tensor. We have found that this moment increases significantly with increasing α . The second application deals with the electromagnetic instabilities driven by the second anisotropy. The stability analysis is performed in the collisionless range without taking into account the saturation effects [22]. The results show that for typical plasmas, strong unstable modes are driven for $\alpha > 0.1$. A more quantitative work of the effects of the IBA on the EDF in strongly-laser-heated plasmas will be done in a future work. Finally a third application related to the influence of strong electric field intensity on photoabsorption is presented. We have found that the non-Maxwellian EDF alters considerably the absorption for moderate and large photon energy with respect to the electron thermal energy.

ACKNOWLEDGMENTS

This work was supported by the Laboratoire Electronique Quantique of Faculty of Physics of USTHB (Bab Ezzouar, Algiers) and the LPGP of Université Paris-Sud 11 (Orsay, France).

-
- [1] J. Dawson and C. Oberman, *Phys. Fluids* **5**, 517 (1962).
 - [2] V. P. Silin, *Zh. Eksp. Teor. Fiz.* **47**, 2254 (1964) [*Sov. Phys. JETP* **20**, 1510 (1965)].
 - [3] W. L. Kruer, *The Physics of Laser Plasma Interaction*, Frontiers in Physics, Vol. 43 (Addison-Wesley, Redwood City, CA, 1973).
 - [4] A. B. Langdon, *Phys. Rev. Lett.* **44**, 575 (1980).
 - [5] P. Mora and H. Yahi, *Phys. Rev. A* **26**, 2259 (1982).
 - [6] J. P. Matte, M. Lamoureux, C. Moller, R. Y. Yin, J. Delettrez, J. Virmont, and T. W. Johnston, *Plasma Phys. Controlled Fusion* **30**, 1665 (1988).
 - [7] A. Bendib, K. Bendib, and A. Sid, *Phys. Rev. E* **55**, 7522 (1997).
 - [8] A. V. Brantov, V. Yu. Bychenkov, V. T. Tikhonchuk, and W. Rozmus, *Phys. Plasmas* **5**, 2742 (1998).
 - [9] A. Tahraoui, A. Bendib, and K. Bendib, *Phys. Plasmas* **7**, 1386 (2000).
 - [10] E. Fourkal, V. Yu. Bychenkov, W. Rozmus, R. Sydora, C. Kirkby, C. E. Capjack, S. H. Glenzer, and H. A. Baldis, *Phys. Plasmas* **8**, 550 (2001).
 - [11] K. Bendib-Kalache, Magister's thesis, Université des Sciences et de la Technologie Houari Boumediène, 1993.
 - [12] R. L. Berger, D. S. Clark, A. A. Solodov, E. J. Valeo and N. J. Fish, *Phys. Plasmas* **11**, 1931 (2004).
 - [13] C. Courtois, A. Couairon, B. Cros, J. R. Marquès, and G. Matthieussent, *Phys. Plasmas* **8**, 3445 (2001).
 - [14] G. Ferrante, M. Zarcone, and S. A. Uryupin, *Phys. Plasmas* **8**, 4745 (2001).
 - [15] M. Lamoureux, C. Möller, and P. Jaeglé, *Phys. Rev. A* **30**, 429 (1984).
 - [16] B. F. Rozsnyai and M. Lamoureux, *J. Quant. Spectrosc. Radiat. Transfer* **43**, 381 (1990).
 - [17] L. Wiesenfeld, *Phys. Lett. A* **144**, 467 (1990).
 - [18] G. M. Fraiman, V. A. Mironov, and A. A. Balakin, *Phys. Rev. Lett.* **82**, 319 (1999).
 - [19] A. Brantov, W. Rozmus, R. Sydora, C. E. Capjack, V. Yu. Bychenkov, and V. T. Tikhonchuk, *Phys. Plasmas* **10**, 3385 (2003).
 - [20] G. Rascol, H. Bachau, V. T. Tikhonchuk, H.-J. Kull, and T. Ristow, *Phys. Plasmas* **13**, 103108 (2006).
 - [21] A. A. Balakin and G. M. Fraiman, *EPL* **93**, 35001 (2011).
 - [22] A. Sangam, J.-P. Morreuw, and V. T. Tikhonchuk, *Phys. Plasmas* **14**, 053111 (2007).
 - [23] E. S. Weibel, *Phys. Rev. Lett.* **2**, 83 (1959).
 - [24] A. Bendib and J. F. Luciani, *Phys. Fluids* **30**, 1353 (1987).
 - [25] I. B. Bernstein, C. E. Max, and J. J. Thomson, *Phys. Fluids* **21**, 905 (1978).
 - [26] H. K. Avetissian, A. G. Chazaryan, H. H. Matevosyan, and G. F. Mkrtchian, *Phys. Rev. E* **92**, 043103 (2015).
 - [27] H. K. Avetissian, A. G. Ghazaryan, and G. F. Mkrtchian, *J. Phys. B: At., Mol. Opt. Phys.* **46**, 205701 (2013).